Additive Manufacturing 51 (2022) 102595

Contents lists available at ScienceDirect

Additive Manufacturing

journal homepage: www.elsevier.com/locate/addma

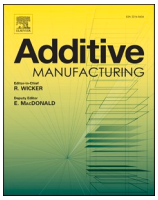

Mold inserts for injection molding prototype applications fabricated via material extrusion additive manufacturing

Anne M. Gohn [a,*], Dylan Brown [a], Gamini Mendis [a], Seth Forster [b], Nathan Rudd [b], Morgan Giles [b]

[a] School of Engineering, Penn State Behrend, 4701 College Drive, Erie, PA 16563, USA
[b] Merck & Co., Inc., Kenilworth, NJ 07033, USA

ARTICLE INFO

Keywords:
Material extrusion
3D printing
Injection molding
Prototype
Product development
Medical plastics

ABSTRACT

As extrusion-based 3D printers are easily accessible and quickly adopted, their application to plastics manufacturing as a prototype development tool continues to expand. In applications where plastic parts are to be injection molded, it is practical to use 3D printing as a tool to prototype and debug the tooling that will be used to mold the desired part. This allows for (1) the functional analysis and debug of the tooling design and (2) the development of injection-molded prototypes, where material properties can be analyzed in the as-manufactured state. In this work, design iterations of extruded 3D printed mold inserts were printed and tested in an injection molding machine to maximize the number of molding cycles before catastrophic damage occurred from the high injection pressures and clamp tonnage. In the optimized design developed in this experiment, 100% infill and a raised shutoff around the part core and cavity allowed for 15 injection molding cycles before the cumulative injection pressures permanently deformed the printed inserts, leading to flashing of the part on the parting line. Mechanical properties show that modulus in the samples molded from the 3D printed tooling insert was lower than that of parts manufactured via extrusion and injection molding using steel tooling, likely due to lower pressure limitations from the 3D printed insert, resulting in a lower density. Surface finish is also noted as an issue when molding parts with the prototype tooling, as the molten material conforms to the valleys between print layers. It is anticipated that prototyping tooling can lower material costs for tooling validation and debug and reduce engineer and equipment time, even if material properties and surface finish of the molded parts are inferior to that of parts molded in steel tooling.

1. Introduction

The application of additive manufacturing (AM) to the tooling design process for injection molding is an advantageous route to new product development. By being able to 3D print prototype injection molding tooling, part designs can be de-bugged before the steel is cut, reducing expensive start-up costs related to steel materials and personnel time. Complex part designs that are difficult to machine can also be trialed with the additive manufacturing process [1]. In addition, injection molded parts can be prototyped to confirm fit, form, and function prior to cutting long-term tooling. The quick-printing capabilities of commercial systems also enables fast turn-around to analyze design modifications with variations to the tooling.

Depending on the printing process, metals, ceramics, and thermoplastic and thermosetting polymers can be used in additive manufacturing. The most common printing technique is extrusion of a thermoplastic polymer strand [2]. In this technique, a traveling extruder head deposits molten plastic in the x and y directions, the printing platform or build stage recedes to allow for new layers in the z direction, and the layers adhere together to form the 3-dimensional printed part. This methodology incorporates a "push" design where a gear box pushes the polymer strand into the heated extrusion head. Compared to thermoset or metal materials, the thermoplastics used in this technique are much more thermally sensitive and can remelt if enough heat is later applied to the printed part, making it troublesome in an injection molding tooling application. However, the technique is inexpensive, more common, and easier to adopt compared to reactive, jetting, or sintering processes [3].

The objective of this work is to create a functioning 3D printed insert to prototype injection molded parts for pharmaceutical applications. Specifically, the goal is to prototype a long-term drug delivery device [4]. These parts are commonly hot-melt extruded to the intended rod

* Corresponding author.
E-mail address: amm6125@psu.edu (A.M. Gohn).

https://doi.org/10.1016/j.addma.2022.102595
Received 4 October 2021; Received in revised form 9 December 2021; Accepted 4 January 2022
Available online 13 January 2022

geometry and cut to length in a secondary process [5–7], but fabrication has also been studied using additive manufacturing [4]. Extruded implant devices currently available on in the market include contraceptives (NuvaRing, Implanon), ophthalmic drugs (Lacrisert®, Ozurdex®), and cancer medications (Zoladex) [8]. Much of the work done in prototyping additively manufactured mold components is not tested using industry's commercially available molding machines [9–11] or the extrusion additive manufacturing process, but has been studied using photopolymerization additive manufacturing processes [12–20].

Relative to the extrusion process, the injection molding process has been found to provide a higher density due to higher pressures in the process [21,22] and higher crystallinity in the polymer matrix [21]. Injection molding also permits for the elimination of secondary processes including cutting the extruded profile to length, broader flexibility with part design beyond the 2-dimensional profile limitation in extrusion, and more efficient scale-up for high production [21] Prototype injection molded parts can be preferred over 3D printed prototypes because in composite applications, the injection molding process significantly impacts the orientation and distribution of the reinforcing agent (fibers, particulates, platelets, etc.), which affects the resulting mechanical properties [23–25]. A drawback of the injection molding process compared to extrusion is the cost of tooling, or the mold used to form and cool the parts [26], which can be mitigated at high production volumes. For this reason, a 3D printed prototype mold insert can be utilized to analyze part efficacy, confirm part design details, and reduce debug time on a steel production mold which can significantly reduce start-up cost and time. It is anticipated that the 3D printed prototype insert will only withstand limited injection molding cycles due to heat and pressure limitations, so this methodology is expected only to be a viable prototyping tool or extremely low-volume production.

The combination of heat and pressure during the injection molding process can cause failure in the 3D printed mold inserts due to yielding and dimensional changes. The compression forces during the injection molding process are influenced by the clamp tonnage of the injection molding press and the injection pressures during the molding process. Clamp tonnages can commonly reach thousands of tonnes and injection pressures commonly range from 70 to 138 MPa [27]. In printing analyses that study compressive strength in extrusion-printed thermoplastic parts, it was found that infill percentage had the largest contributions to increased compressive force [28,29], and more shell layers yielded higher compressive strength [28]. Dimensional accuracy, which is critical to obtaining a smooth surface finish in injection molded parts, was found to increase when layer height decreased [30]; however, decreased layer height also contributed to a decreased compressive strength [28]. In this work, 3D printed mold inserts are fabricated using a series of design changes to injection mold medical device implants. Permament deformation of the mold, resulting in flash, is studied over repeated injection cycles, to identify the most effective design parameters for creating durable mold inserts. Moldflow simulations are performed to identify the expected pressure distributions during molding. The resulting injection molded implants are characterized to understand resulting crystallinity and mechanical properties to evaluate the quality of the parts when compared with conventionally manufactured parts. The contributions of printing parameters to part properties are discussed [28].

2. Materials and methods

2.1. Instrumentation

2.1.1. 3D printing

Material extrusion 3D printing was performed on an Ultimaker 3. Polyamide 6 (PA 6) was used as the 3D printing filament due to its high melting temperature relative to other commercially available 3D printing filaments. Neat PA 6 (MatterHackers Pro Series Nylon) and 12.5 wt% carbon fiber filled PA 6 (PA6/CF) (CarbonX from 3DXTECH) [31] at 2.85 mm diameter were selected as commercially available filaments for the printing of the injection mold inserts. Prior to printing, the filament was dried for 4 h at 75 °C in a desiccant oven. Bed and nozzle temperatures were set to 75 °C and 270 °C, respectively, per the filament supplier recommendations. The material flow rate was set to 100% and layer height was set to 0.2 mm. A nozzle diameter of 0.4 mm and print speed of 70 mm/s was used. A flat (x, y) build orientation was used to print each mold insert, and the specific infill conditions are listed with each design iteration. The printed insert geometry for all infill conditions is comprised of 35 mm height and 110 mm length, and the cylinder part cavity is a cylinder with 40 mm length and 2 mm diameter. (Figs. 1, 2).

2.1.2. Injection molding

Injection molding was performed on a BOY XS molding machine equipped with a 12 mm screw diameter, 19.7 L/D ratio, and 50 mm diameter barrel. Ateva® ethylene vinyl acetate (EVA) 1070 from Celanese was used as the polymer for injection molding [5,6]. Optimized process settings were developed using steel mold inserts with the identical geometry of the 3D printed inserts in order to establish the process. It was determined that parts could be produced using a 14 mm shot size and 7 mm transfer position with an injection velocity of 20 mm/s. Transfer to hold pressure (5.5 MPa) was set to occur when the part was filled 95% from shot size alone to accommodate for shrinkage during solidification from the melt [32]. A 20 s cooling time was set prior to manual part picking. A barrel temperature of 180 °C for the EVA was used. Mold cooling was not printed into the insert parts to prevent water leakage, so tool temperature was at ambient conditions. An example of a set of machined steel inserts in the cavity and core plates are displayed in Fig. 3. Samples were molded using the steel inserts as a baseline for comparison to the 3D printed inserts.

2.1.3. Extrusion

Extrusion of the implant geometry was used as a baseline for

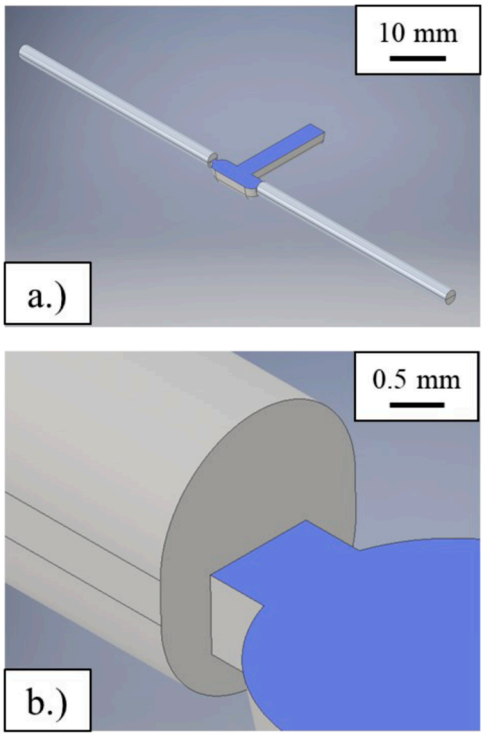

Fig. 1. Part geometry replicating the pharmaceutical implant Nexplanon (Organon & Co., Jersey City, NJ, USA) (a) and the tab gate transition from runner to part (b).

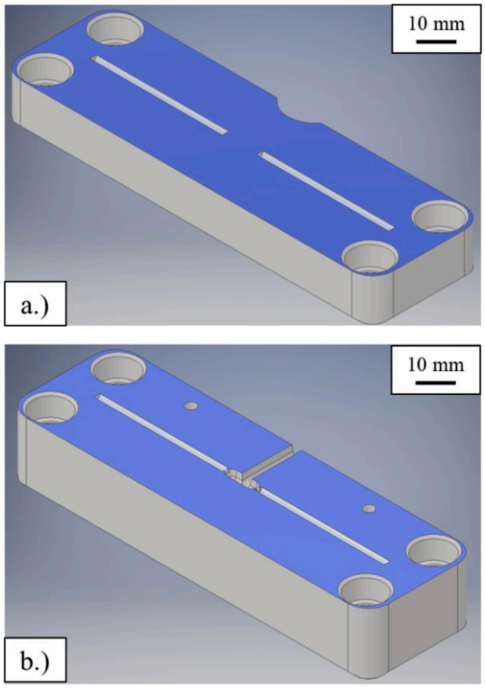

Fig. 2. Mold insert core (a) and cavity (b) part files to create the implant geometry.

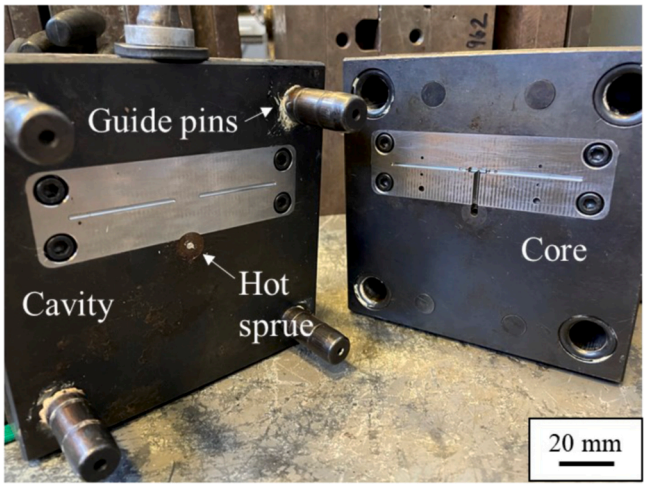

Fig. 3. Mold inserts installed in cavity and core plates for injection molding.

resulting sample characterization. EVA samples were extruded on a Brabender Plasticorder Rheometer with a 3 mm round die. The extruder is equipped with a 19 mm screw, 30:1 L/D ratio, and 3:1 compression ratio. Extrusion was performed at 180 °C and 50 RPM. Once material was extruded out of the die, the strand was drawn down to 2 mm diameter through a water bath using a puller.

2.1.4. Differential scanning calorimetry (DSC)

DSC analysis was performed on a Mettler Toledo DSC 1 to analyze the melting temperatures of the EVA and PA 6 used in this study. To meet the objectives of this work, the processing melt temperature of the EVA needs to be lower than the melting point of the PA 6 to ensure the thermal stability of the insert is constant throughout the molding process. Samples were heated at 10 °C/min to 180 °C and 250 °C for the EVA and PA 6, respectively. The polymer was then held at that temperature for 3 min to ensure equilibrium was reached, followed by cooling at 10 °C/min to a minimum temperature of 0 and 25 °C for the EVA and PA 6, respectively. The heat/cool cycle was then repeated a second time. To analyze the crystal fraction in the manufactured EVA samples, the same calorimetric protocol was applied, but the melting peak of the first heating scan was analyzed. A nitrogen purge of 30 mL/min was used for all measurements to prevent sample oxidation.

2.1.5. Mechanical testing

Compression testing was performed to quantify forces required to permanently deform the printed mold inserts. A Tinius Olsen universal testing machine was employed at 5 mm/min compressive rate. Samples were prepared by 3D printing sample blocks (40 mm × 40 mm × 40 mm) at similar print conditions to the injection molding insert designs (4 layer shell). Compression samples were printed using neat PA 6 at 30% infill, PA 6/CF at 30% infill, and PA 6/CF at 100% infill to mimic the print parameters used in the insert design sequence. Tensile testing was used to compare mechanical properties of the parts manufactured under the different methods. Testing was performed on a Tinius Olsen 25ST at 4 mm/min. 3 samples of each manufacturing condition were tested.

2.1.6. Mold filling simulation

Mold filling simulation was used to determine injection pressures anticipated from the injection molding process imposed on the 3D printed inserts. Autodesk Moldflow Insight 2021 software was used for the analysis. The part geometry was imported into the software, and a 3D mesh was created using 11 elements through the thickness of the part, yielding 254,000 total elements in the part file. The Fill+Pack analysis sequence was run using Greenflex ML30 EVA from Versalis in the Autodesk Moldflow database since the specific grade of EVA used in this study was not available. The vinyl acetate (VA) contents are the same at 9%, and melt flow viscosities of the materials are similar, at 2.5 and 2.8 for Greenflex mL 30 and Ateva 1070, respectively, so these parameters are expected to be sufficiently representative to model the specific grade used in this study. The analysis was performed using the actual injection molding conditions used to mold samples in this process.

2.1.7. Scanning electron microscopy (SEM)

SEM was performed to capture the surface finish of parts created under differing manufacturing conditions. Micrographs of the as-manufactured part surfaces were captured using a FEI Quanta 650. Imaging of the unmodified surfaces was performed using a spot size of 4.5, a 10 kV accelerating voltage, and a chamber pressure of 40 Pa.

3. Results and discussion

The melting temperatures were analyzed by DSC to confirm the temperatures chosen for the EVA molten polymer and the injection molding machine's hot sprue would not melt the printed inserts. The heat flow signals as a function of temperature are shown in Fig. 4. The second heating cycle is displayed to show the subsequent melting after a known, consistent cooling profile. Endothermic peaks in this analysis indicate crystal fraction melting. The EVA shows melting onset begins at approximately 15 °C, and the peak melting temperature (T_m) occurs at 99 °C. Both PA 6 filaments show bimodal melting peaks, which indicates polymorphic crystal development and reorganization to the more stable crystal form in the as-solidified samples [33–35]. The neat PA 6 filament is slightly less thermally stable than the CF PA 6 with bimodal T_m at 189 °C and 198 °C. The CF reinforced PA 6 filament displays bimodal T_m at 208 and 218 °C. From this analysis, it was determined that using an EVA melt temperature of 180 °C per the resin supplier [36] would be low enough to avoid melting the printed PA 6 inserts, though it was anticipated the neat PA 6 would have a higher degree of softening than the CF reinforced PA 6. The glass transition temperature (T_g) of PA 6 has been reported to occur between 66 °C and 77 °C depending on the crystallization conditions [37], so it is anticipated the insert may have

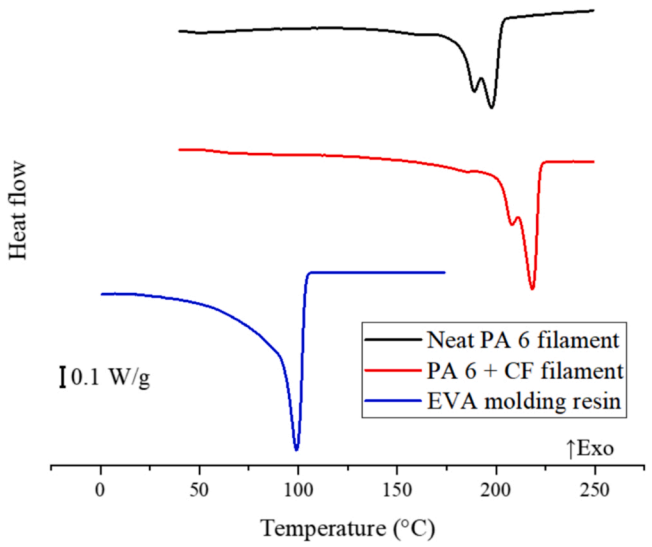

Fig. 4. Calorimetry of neat PA 6 filament, carbon fiber filled PA 6 filament, and EVA molding resin to analyze critical melting ranges. Samples have been normalized to sample mass and melting profiles are obtained at 10 °C/min heating rate.

additional ductility when exposed to the processing temperature of EVA, though it will still be in solid phase.

3.1. Insert design 1: neat PA 6, 30% gyroid infill

The neat PA 6 grade was used to print the first core and cavity inserts for the experiment. A 30% infill using the gyroid pattern was selected for this first design iteration, as shown in Fig. 5a. The printed insert is displayed in Fig. 5b. Parts resulting from the injection molding process are displayed in Fig. 5c. For each injection cycle, the parts are labeled as Cycle 1, Cycle 2, etc. to indicate the progression of the consecutive parts molded using the printed tooling. After only 3 cycles, it is shown that the injection forces caused permanent deformation of the printed insert, which then caused molding flash, or excess material adhered to the part at the parting line of the mold between the inserts. With each additional injection molding cycle, each part continuously proceeded to develop more flash, indicating that additional deformation was occurring in the printed insert. It was decided a material with higher compressive strength and a higher infill would be needed in this region to overcome the injection pressures needed in the molding process. Due to high flash and poor process stability, it was determined that no parts were practical for prototype use.

3.2. Insert design 2: PA6/CF, 30% triangular infill with local 100% infill region

In the second design iteration, a local section of 100% infill using line pattern was added to overcome 3D printed insert deformation observed in Design 1. The 30% infill using triangular pattern was used throughout the remainder of the insert to try to reduce material, as shown in Fig. 6a. An image of the printed core insert after the molding attempt is displayed in Fig. 6b and shows the permanent deformation was moved to the area outside of the 100% local infill region. The injection molding cycle progression in Fig. 6c displays that with each additional molding cycle, the flash continuously worsened in the region outside the local dense infill. Regarding the viability of the molded parts from this printed insert, it was again determined that no parts were practical for prototype use.

3.3. Insert design 3: PA6/CF, 100% line infill

To overcome the deformation issues in design iterations 1 and 2, it was decided that 100% infill through the full part would be necessary to overcome the injection pressures that cause deformation, resulting in flash on the molded parts. The print cross section and the printed cavity after used in the injection molding process are displayed in Fig. 7a and Fig. 7b, respectively. The injection molding cycle progression from cycle 2 through 9 are displayed in Fig. 7c, showing that the major flash issues seen in insert designs 1 and 2 is much improved at the higher infill density, which relates to a higher compressive strength. From this insert, approximately 7–9 prototypes with mild flash at the parting line can be

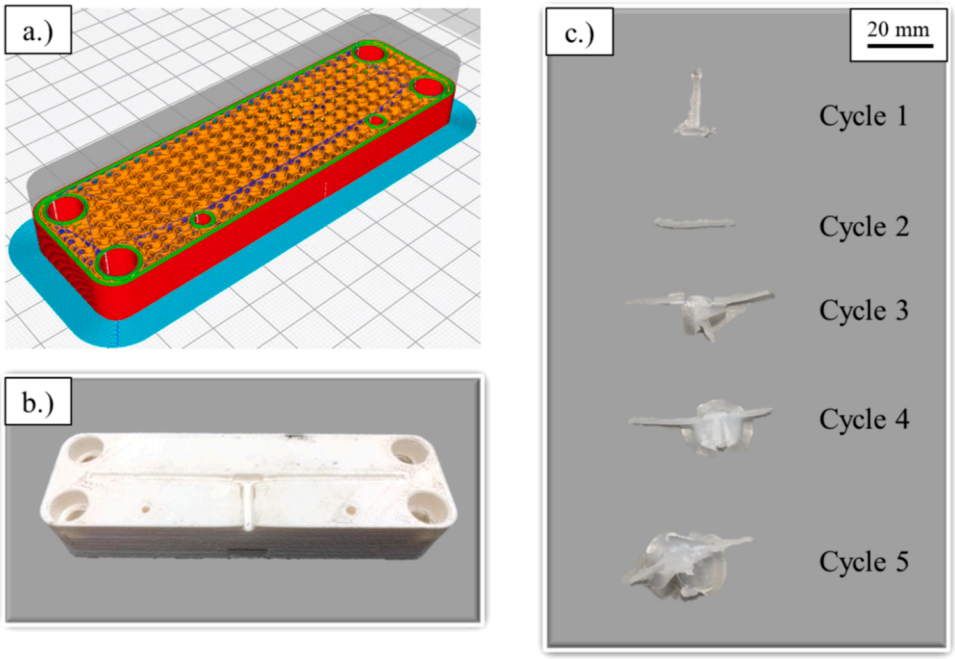

Fig. 5. Insert design 1 displaying 30% infill using gyroid pattern (a), the printed insert (b), and the injection molding cycle progression forming molded parts using the insert (c).

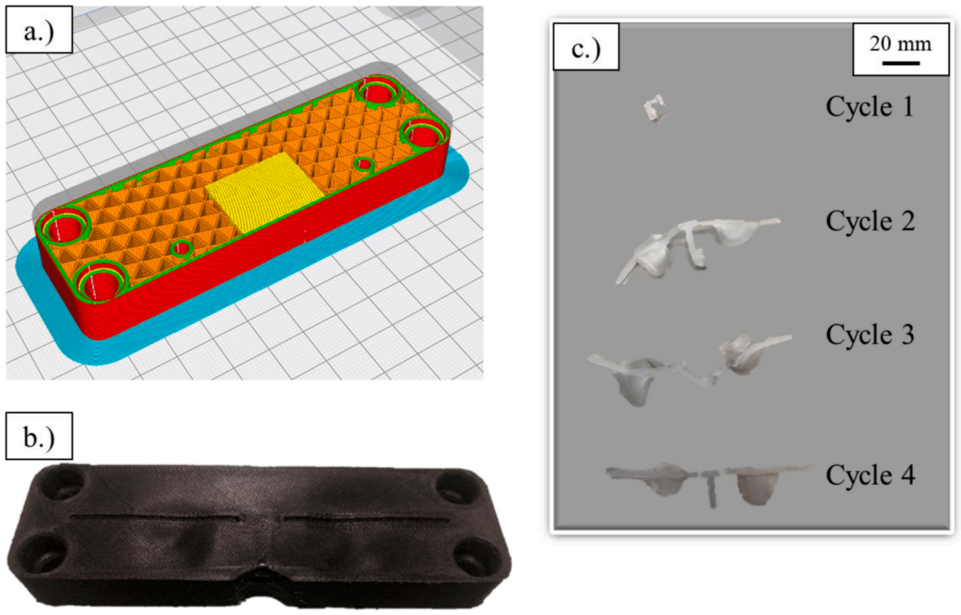

Fig. 6. Insert design 2 displaying 100% infill at the local region that displayed permanent deformation in Design 1% and 30% infill using gyroid pattern throughout the remainder of the insert (a), the printed insert after molding displaying regions of permanent deformation (b), and the injection molding cycle progression forming molded parts using the insert (c).

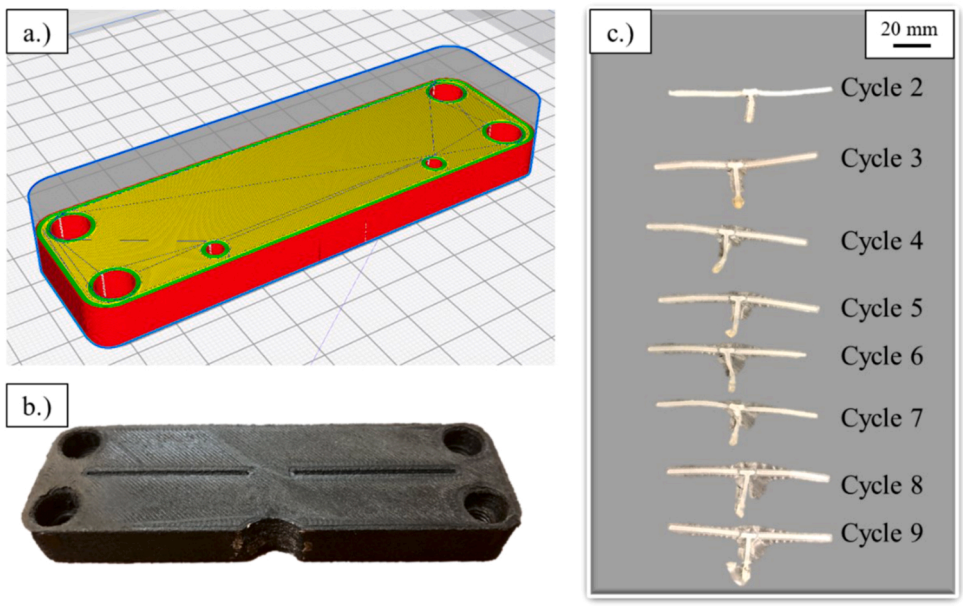

Fig. 7. Insert design 3 displaying 100% infill using line pattern throughout the whole insert (a), the printed insert (b), and the injection molding cycle progress (c).

achieved before the cumulative injection pressures cause permanent deformation to the insert, resulting in ineffective prototypes. Ramesh et al. found that in a material extrusion printing study, polyamide parts with 100% infill density had the most impactful contribution to increasing the flexural strength, tensile strength, impact strength, and hardness due to lower number of voids to permit for crack propagation when the different load mechanisms were applied [29].

3.4. Insert design 4: PA6/CF, 100% line infill with raised shutoff

The fourth design iteration included a raised shut-off around the runner and part with a width of 2 mm and a thickness of one printed layer height (0.2 mm). The added height required stopped flash for the first twelve molding cycles and only produced minimal flash until over 15 injection molding cycles. Any flash that did occur only affected the runner and not the parts in the molded prototypes. In this design iteration, it is assumed that at least 15 prototypes can be injection molded before flash at the parting line becomes a major issue that affects the integrity of the part. It is also notable that during manual part pulling, some of the parts de-gated, as shown in Fig. 8c.

3.5. Cavity pressure requirements

Mold filling simulation was performed using the part geometry and injection molding conditions to predict injection pressures developed during the molding process. The end of the hot sprue was modeled as the injection location into the part geometry. The pressure as a function of the part geometry is shown in Fig. 9, which was captured at (a) the point

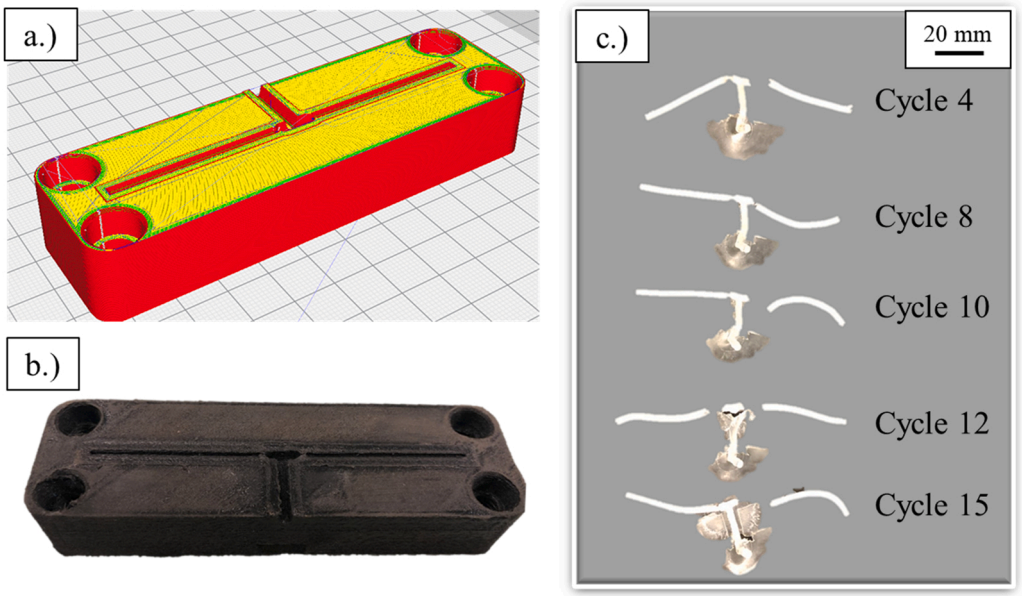

Fig. 8. Insert design 4 displaying 100% infill using line pattern throughout the whole insert and a raised shutoff around the part core and cavity (a), the printed insert after the molding trial (b), and the injection molding cycle progress (c).

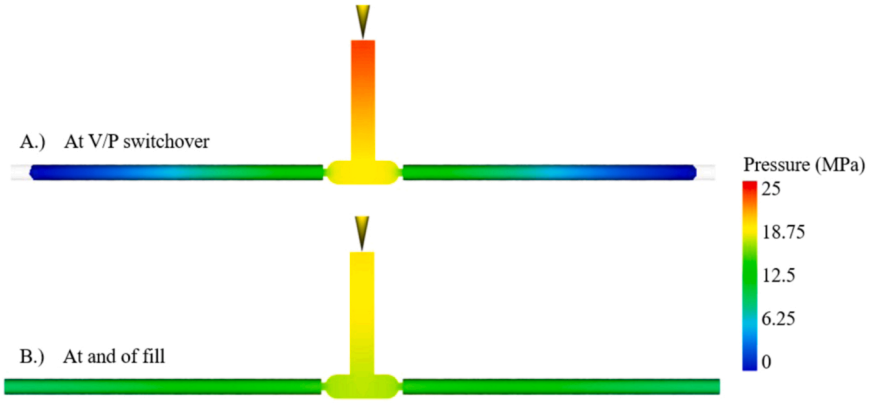

Fig. 9. Mold filling simulation pressure prediction at (a) V/P switchover when the part-filling process transitions from fill by injection to hold pressure and (b) when the part is completely filled.

of velocity to hold pressure switchover and (b) at the time the cavity is filled. The maximum injection pressure is approximately 25 MPa, which is developed in the runner of the part. The pressures in the gate reaches a maximum of about 12.5 MPa, with the part geometry having the lowest injection pressure during the process. Flash, caused by permanent deformation of the insert, occurs first in the runner before the part geometry in the molded prototypes, which agrees with the pressure simulation shown here. Deformation occurs first at the points of highest pressure and worsens with each injection cycle due to cumulative forces.

Compression testing of 3D printed sample blocks was performed to analyze if compression loading of test specimens printed at the conditions used for the mold insert could be correlated with failures associated with deformation from injection pressures during the molding cycle. Raw data from the compression tests at the different print designs are displayed in Fig. 10. The mechanical test confirms that the carbon fibers increase the compressive strength compared to that of the neat PA 6 material. However, the 30% infill design, regardless of neat or carbon fiber filled, compressive strength is lower than 25 MPa, which is the expected maximum pressure developed during plastic injection during the molding cycle. This result confirms the immediate deformation developed in the insert Designs 1, 2, and 3. The carbon fiber filled PA 6 specimen printed at 100% infill shows plastic deformation occurs at approximately 60 MPa, which is greater than the injection pressure to be applied during the injection molding process. However, some flash was still developed around the parting line of the part in Insert Design 4. This leads the authors to believe the seal between the cavity and core inserts is difficult to maintain in extrusion-based additive manufacturing, as air gaps exist between the rasters [38] and interfacial voids can occur if print conditions are not optimized [39]. If void content is present, the polymer can easily flow into areas where print design permits.

3.6. Property comparison

To analyze the resulting properties of the injection molded prototypes, implant samples were characterized after manufactured via (1) extrusion, (2) injection molding using the standard steel insert, and (3) injection molding using the optimized 3D printed insert with shutoff around the cavity and core geometry. A macroscopic image of the samples after their fabrication is shown in Fig. 11. It can be seen that the injection molded sample using the steel insert and the extruded sample have very smooth surface finishes, producing an optically transparent specimen, while the rough surface of the sample injection molded using

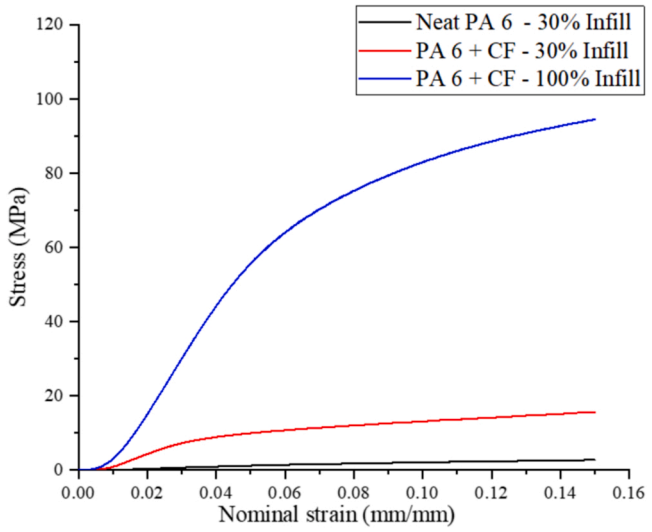

Fig. 10. Compression testing of samples mimicking the 3D printed mold inserts to analyze compressive properties of the bulk parts.

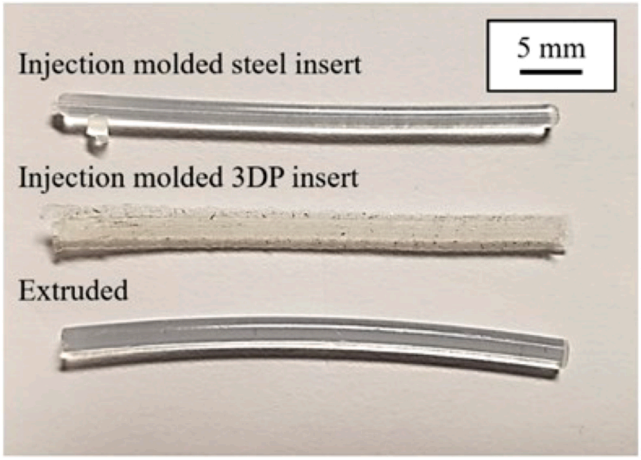

Fig. 11. Macroscopic imaging of samples fabricated via injection molding with a steel insert, injection molding with a 3D printed insert (molded using Design 4 – 100% infill with shutoff), and extrusion.

the 3D printed inserts have a course surface finish, producing an opaque part. Though the surface finish is courser, the desired part geometry is still maintained, and the part was analyzed for mechanical integrity.

The resulting crystallinity was measured by integrating the melting peak on the first heating scan. Samples were taken as a full cross-sectional area, and molded samples were taken from the part's end of fill location. To determine crystallinity, a heat of fusion of 293 J/g of pure polyethylene was used [40], and integration limits from 60 °C to 115 °C were applied for each sample. Absolute crystallinity values of 30.9%, 21.3%, and 28.5% were calculated for the samples that were injection molded using the 3D printed insert, injection molded using the steel insert, and extruded, respectively. The low as-molded crystallinity value in the injection molded sample using the steel insert is due to the high cooling rate quench where the molten plastic meets the thermally conductive steel mold wall. The highest crystallinity value is obtained in the sample molded using the 3D printed insert, where there is low thermal conductivity, and the part is able to cool more slowly, yielding a higher crystallinity value. (Fig. 12).

Surface finish of the implant rods were characterized using electron microscopy. Fig. 13 shows the surface finish of samples created by (a) injection molding using the 3D printed insert, (b) injection molding

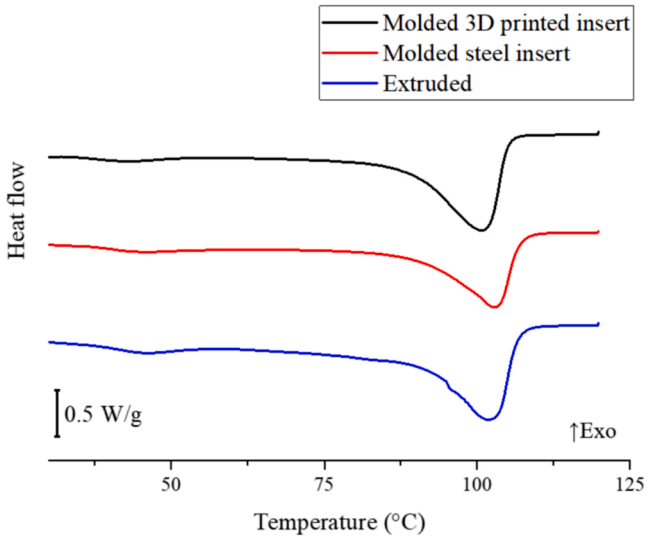

Fig. 12. DSC first heating curves of EVA manufactured via injection molding with the 3D printed insert (top, black), injection molding with a steel insert (middle, red), and extruded (bottom, blue). (For interpretation of the references to color in this figure, the reader is referred to the web version of this article.)

using the steel insert, and (c) extruded. The surface finish is smoothest by manufacturing using the steel injection molding insert, as the plastic takes the surface texture of the machining conditions used to manufacture the insert. Extrusion also produced a smooth surface finish, though slightly more defects are present from the extrusion process, where material is affected by die finish, rollers in the water bath, and the puller while still malleable. Significantly rougher surface finish is produced when injection molding into the 3D printed insert, where the polymer material tries to fill boundaries between surface print layers, known as valleys. Fig. 13d displays a schematic of the deposited beads during the 3D printing process. Between the beads internal to the printed parts, voids may be present due to the circular shape of the extrusion nozzle. This effect at the surface is denoted as a valley. During the injection molding process, the injected molten material will fill the valleys, producing surface defects up to 0.1 mm.There also appears to be a ductile "pulling" mechanism at the surface, which can be an attribute of the EVA sticking to the PA 6 mold insert and is permanently deformed when ejected from the mold.

Tensile properties were evaluated of the implant specimens manufactured via injection molding using the 3D printed insert, injection molding using the steel insert, and extrusion. Raw data and data summaries are depicted in Fig. 14. Representative raw data curves for each manufacturing set are displayed in Fig. 14A. It is shown that a higher stress at yield and break is obtainable in the extruded and injection molded in steel samples compared to that of the 3D printed insert. Fig. 14B displays average strain at break for each manufacturing method. The extruded samples proved to have the largest strain at break. The modulus of the samples that were extruded and injection molded using the steel insert are similar but is lowest in the samples injection molded using the 3D printed inserts. It is concluded that the high extension exhibited in the extruded samples is a result of the high degree of orientation achieved from the extrusion process. The modulus is a correlation to the density of the fabricated parts depending on the manufacturing process. The densities of the extruded samples and samples injection molded using the steel inerts are expected to be the highest, and lowest in the injection molded samples using the 3D printed insert. The tensile properties studied here are dictated by the density and degree of orientation more than the degree of crystallinity.

Though the surface finish and tensile properties are not equivalent to those manufactured via extrusion or traditional injection molding using a steel insert, the use of an additively manufactured insert for prototype

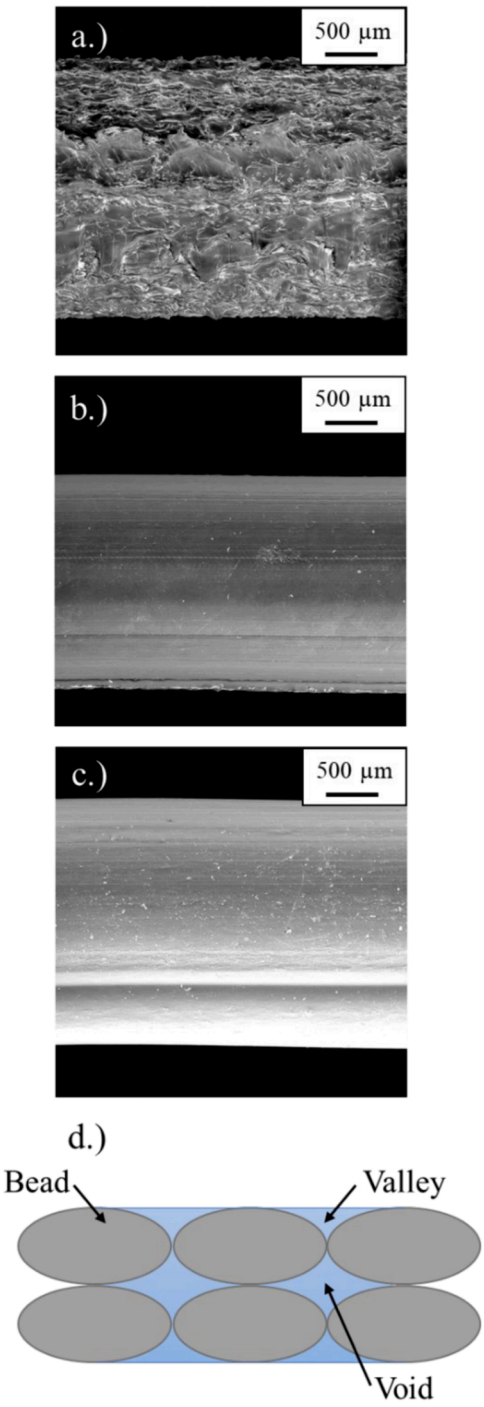

Fig. 13. Electron microscopy of surface finish of samples prepared via injection molding with the 3D printed insert (a), injection molding with a steel insert (b), and extruded (c). A schematic describing the surface effects from the 3d printing process is shown in (d), where the material bead from the extrusion process is gray, and blue indicates void space between beads. Void space on the surface of the printed part is designated as a valley. (For interpretation of the references to color in this figure, the reader is referred to the web version of this article.)

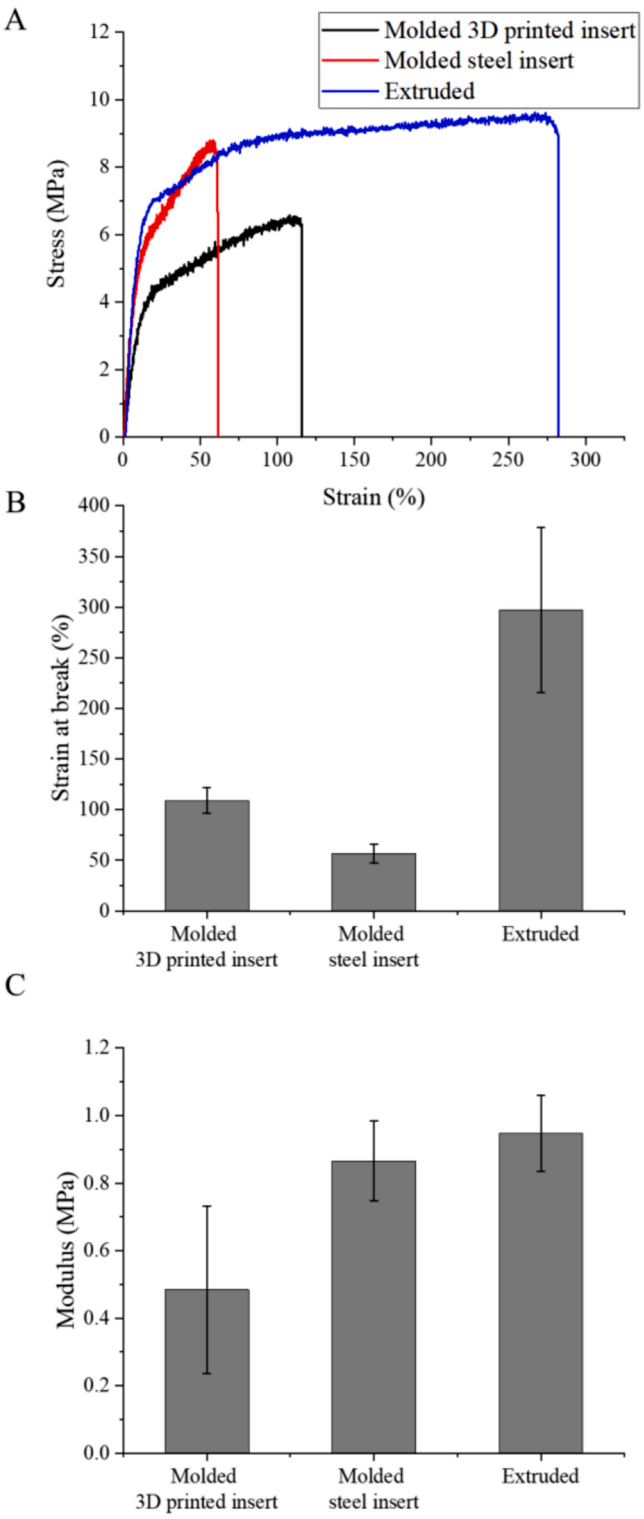

Fig. 14. Tensile properties of implant samples prepared via injection molding with 3D printed insert, injection molding with steel insert, and extrusion. Raw data of representative curves (A), average strain at break (B), and average modulus (C), where error bars indicate one standard deviation.

parts is still seen as an advantageous route for prototyping injection molded parts. For example, composite systems can be analyzed for filler/additive/reinforcing agent orientation as impacted by the manufacturing conditions, flow patterns can be analyzed to better determine weld line locations, and molded prototypes can be used to determine appropriate venting locations. By analyzing the injection molding considerations in a prototype tool, money and time can be saved during de-bug efforts, where often times these corrections need completed on steel tooling.

4. Conclusions

The development of injection molding tooling can be an expensive endeavor, where the tooling itself is costly and often requires adjustments after a validation period. By prototyping injection molding tooling, engineers can (1) reduce the time and material costs of debugging a steel mold and (2) prototype the injection molded part to study manufacturing-specific material considerations. This experiment systematically analyzes extrusion-based 3D printed injection molding inserts for optimizing cycles in the injection molding machine. It was found that the PA 6/CF composite material was needed for its structural integrity, and that 100% infill with a raised shutoff around the part's cavity and core allowed for the maximum number of usable parts. In this design scheme, 15 functioning parts were able to be collected before the injection pressures of the molding process caused permanent deformation in the insert, which contributed to the flash defect development along the parting line of the part. As material extrusion is the most common and inexpensive of the additive manufacturing techniques, it is anticipated that prototype tooling can be easily applied to new product development to save companies time and money in process start-up.

Physical, mechanical, and morphological properties of samples manufactured via extrusion, molded using a 3D printed insert, and molded using a steel insert were analyzed. It was found that rough surface finish was produced in parts molded in the 3D printed insert, as the hot melt conforms to the valleys between print beads. The molded EVA polymer also appears to have ductile "pulling" areas on the surface, noting that the material wanted to stick to the PA 6 core and was deformed when manually ejected. The modulus of the extruded samples is 84% greater than that of samples molded in the 3D printed parts, which can be related to the final density attainable from each manufacturing technique. Though the mechanical properties and surface finish of the parts manufactured via additively manufactured plastic tooling, the use of 3D printed thermoplastic tooling can be successful to prototype injection molding tooling and to prototype injection molded parts at low cost and fast response time. The injection molded prototype parts can allow engineers to better determine flow patterns in the molded parts, which affect reinforcing agent, filler, and additive orientation and thus, mechanical properties. From a tooling perspective, the ability to injection mold into prototype tooling will allow for design debug related to weld line locations, proper venting design pending actual flow patterns, and optimized runner/gate geometries.

CRediT authorship contribution statement

Anne M Gohn: Writing – review & editing, Methodology, Supervision, Funding acquisition, Formal analysis, Data curation, Conceptualization. **Dylan Brown:** Investigation, Data curation. **Gamini Mendis:** Writing – review & editing. **Seth Forster:** Writing – review & editing, Funding acquisition. **Nathan Rudd:** Writing – review & editing. **Morgan Giles:** Writing – Review & Editing.

Declaration of Competing Interest

The authors declare the following financial interests/personal relationships which may be considered as potential competing interests: Anne M. Gohn reports financial support was provided by Pennsylvania Department of Community and Economic Development Manufacturing PA Innovation Program. Anne M. Gohn reports financial support was provided by Merck Sharp & Dohme Corp., a subsidiary of Merck & Co., Inc., Kenilworth, NJ, USA.

Acknowledgments

This work was financially supported by the Pennsylvania Department of Community and Economic Development Manufacturing PA Innovation Program and Merck Sharp & Dohme Corp., a subsidiary of Merck & Co., Inc., Kenilworth, NJ, USA. The authors would also like to thank David Peterson, Ethan Ravotti, Amy Nolte, and Chris Bartlett from Pennsylvania State University for their technical support.

References

[1] H.S. Park, X.P. Dang, Development of a smart plastic injection mold with conformal cooling channels, Procedia Manuf. 10 (2017) 48–59, https://doi.org/10.1016/j.promfg.2017.07.020.
[2] J.C. Najmon, S. Raeisi, A. Tovar, Review of additive manufacturing technologies and applications in the aerospace industry, Addit. Manuf. Aerosp. Ind. (2019) 7–31, https://doi.org/10.1016/B978-0-12-814062-8.00002-9.
[3] Z. Jiang, B. Diggle, M.L. Tan, J. Viktorova, C.W. Bennett, L.A. Connal, Extrusion 3D printing of polymeric materials with advanced properties, Adv. Sci. 7 (2020) 1–32, https://doi.org/10.1002/advs.202001379.
[4] N. Genina, J. Holländer, H. Jukarainen, E. Mäkilä, J. Salonen, N. Sandler, Ethylene vinyl acetate (EVA) as a new drug carrier for 3D printed medical drug delivery devices, Eur. J. Pharm. Sci. 90 (2016) 53–63, https://doi.org/10.1016/j.ejps.2015.11.005.
[5] S.E. Barrett, R.S. Teller, S.P. Forster, L. Li, M.A. Mackey, D. Skomski, Z. Yang, K. L. Fillgrove, G.J. Doto, S.L. Wood, J. Lebron, J.A. Grobler, R.I. Sanchez, Z. Liu, B. Lu, T. Niu, L. Sun, M.E. Gindy, Extended-duration MK-8591-eluting implant as a candidate for HIV treatment and prevention, Antimicrob. Agents Chemother. 62 (2018), https://doi.org/10.1128/AAC.01058-18.
[6] C. Schneider, R. Langer, D. Loveday, D. Hair, Applications of ethylene vinyl acetate copolymers (EVA) in drug delivery systems, J. Control. Releas. 262 (28) (2017) 284–295. https://www.sciencedirect.com/science/article/pii/S016836591730771X.
[7] D. Skomski, Z. Liu, Y. Su, C.T. John, A. Doty, S.P. Forster, R. Teller, S.E. Barrett, W. Xu, An imaging toolkit for physical characterization of long-acting pharmaceutical implants, J. Pharm. Sci. 109 (2020) 2798–2811, https://doi.org/10.1016/j.xphs.2020.05.031.
[8] C. Brown, J. DiNunzio, M. Eglesia, S. Forster, M. Lamm, M. Lowinger, P. Marsac, C. McKelvey, R. Meyer, L. Schenck, G. Terife, G. Troup, B. Smith-Goettler, C. Starbuck, Hot-melt extrusion for solid dispersions: composition and design considerations, Amorph. Solid Dispers. (2014) 197–230, https://doi.org/10.1007/978-1-4939-1598-9_6.
[9] J.R.C. Dizon, A.D. Valino, L.R. Souza, A.H. Espera, Q. Chen, R.C. Advincula, 3D printed injection molds using various 3D printing technologies, Mater. Sci. Forum 1005 MSF (2020) 150–156, https://doi.org/10.4028/www.scientific.net/MSF.1005.150.
[10] P. Chung, J.A. Heller, M. Etemadi, P.E. Ottoson, J.A. Liu, L. Rand, S. Roy, Rapid and low-cost prototyping of medical devices using 3D printed molds for liquid injection molding, J. Vis. Exp. (2014) 1–16, https://doi.org/10.3791/51745.
[11] F. Rayegani, G.C. Onwubolu, A. Nagy, H. Singh, Functional prototyping and tooling of FDM additive manufactured parts, ASME Int. Mech. Eng. Congr. Expo. Proc. (2014) 1–7, https://doi.org/10.1115/IMECE2014-37828.
[12] J. Noble, K. Walczak, D. Dornfeld, Rapid tooling injection molded prototypes: a case study in artificial photosynthesis technology, Procedia CIRP 14 (2014) 251–256, https://doi.org/10.1016/j.procir.2014.03.035.
[13] M. Mischkot, G. Tosello, D.K.Y. Nielsen, D.B. Pedersen, Y. Zhang, T. Hofstätter, L. Herbin, H.N. Hansen, Injection moulding pilot production: performance assessment of tooling process chains based on tool inserts made from brass and a 3D printed photopolymer, Annu. Tech. Conf. ANTEC Conf. Proc. (2017) 1898–1902.
[14] K. Altaf, J.A. Qayyum, A.M.A. Rani, F. Ahmad, P.S.M. Megat-Yusoff, M. Baharom, A.R.A. Aziz, M. Jahanzaib, R.M. German, Performance analysis of enhanced 3D printed polymer molds for metal injection molding process, Metals 8 (2018) 433, https://doi.org/10.3390/met8060433.
[15] E. Sachs, E. Wylonis, S. Allen, M. Cima, H. Guo, Production of injection molding tooling with conformal cooling channels using the three dimensional printing process, Polym. Eng. Sci. 40 (2000) 1232–1247, https://doi.org/10.1002/pen.11251.
[16] P. Simpson, A.D. Zakula, J. Nelson, J.K. Dworshak, E.M. Johnson, C.A. Ulven, Injection molding with an additive manufactured tool, Polym. Eng. Sci. 59 (2019) 1911–1918, https://doi.org/10.1002/pen.25192.
[17] T. Mitterlehner, C. Beisteiner, H. Rieger, P. Dunzendorfer, G. Steinbichler, Back injection molding with additive manufactured mold inserts using all-inkjet printed substrates, Annu. Tech. Conf. ANTEC, Conf. Proc. (2017) 7–12.
[18] S. Krizsma, N.K. Kovács, J.G. Kovács, A. Suplicz, In-situ monitoring of deformation in rapid prototyped injection molds, Addit. Manuf. 42 (2021), 102001, https://doi.org/10.1016/j.addma.2021.102001.
[19] G. Schuh, G. Bergweiler, G. Lukas, J.A. Abrams, Feasibility and process capability of polymer additive injection molds with slide technology, Procedia CIRP 93 (2020) 102–107, https://doi.org/10.1016/j.procir.2020.03.057.
[20] Q. Saby, J.Y. Buffière, E. Maire, T. Joffre, J. Bajolet, S. Garabédian, P. Vikner, X. Boulnat, Laser powder bed fusion printability of cobalt-free steel powders for manufacturing injection molds, Addit. Manuf. 44 (2021), 102031, https://doi.org/10.1016/j.addma.2021.102031.
[21] A. Rothen-Weinhold, K. Besseghir, E. Vuaridel, E. Sublet, N. Oudry, F. Kubel, R. Gurny, Injection-molding versus extrusion as manufacturing technique for the preparation of biodegradable implants, Eur. J. Pharm. Biopharm. 48 (1999) 113–121, https://doi.org/10.1016/S0939-6411(99)00034-X.

[22] A. Melocchi, G. Loreti, M.D. Del Curto, A. Maroni, A. Gazzaniga, L. Zema, Evaluation of hot-melt extrusion and injection molding for continuous manufacturing of immediate-release tablets, J. Pharm. Sci. 104 (2015) 1971–1980, https://doi.org/10.1002/jps.24419.
[23] P. Shokri, N. Bhatnagar, Effect of packing pressure on fiber orientation in injection molding of fiber-reinforced thermoplastics, Polym. Compos. 28 (2007) 214–223.
[24] M. Gupta, K.K. Wang, Fiber orientation and mechanical properties of short-riber-teinforced injection-molded composites: simulated and experimental results, Polym, Composites 40 (1994) 799–812.
[25] H.C. Tseng, R.Y. Chang, C.H. Hsu, Numerical predictions of fiber orientation and mechanical properties for injection-molded long-glass-fiber thermoplastic composites, Compos. Sci. Technol. 150 (2017) 181–186, https://doi.org/10.1016/j.compscitech.2017.07.026.
[26] D.V. Rosato, M.G. Rosato, Injection Molding Handbook, third ed., Springer, Boston, MA, 2001.
[27] T.A. Osswald, L.S. Turng, P. Gramann, Injection Molding Handbook, Hanser Gardner Publications, Inc., Cincinatti, OH, 2008.
[28] U.K. uz Zaman, E. Boesch, A. Siadat, M. Rivette, A.A. Baqai, Impact of fused deposition modeling (FDM) process parameters on strength of built parts using Taguchi's design of experiments, Int. J. Adv. Manuf. Technol. 101 (2019) 1215–1226, https://doi.org/10.1007/s00170-018-3014-6.
[29] M. Ramesh, K. Panneerselvam, Mechanical investigation and optimization of parameter selection for Nylon material processed by FDM, Mater. Today Proc. (2020) 9303–9307, https://doi.org/10.1016/j.matpr.2020.02.697.
[30] C.K. Basavaraj, M. Vishwas, Studies on effect of fused deposition modelling process parameters on ultimate tensile strength and dimensional accuracy of nylon, IOP Conf. Ser. Mater. Sci. Eng. 149 (2016), 012035, https://doi.org/10.1088/1757-899X/149/1/012035.
[31] P. Striemann, S. Bulach, D. Hülsbusch, M. Niedermeier, F. Walther, Shear characterization of additively manufactured short carbon fiber-reinforced polymer, Macromol. Symp. 395 (2021) 1–5, https://doi.org/10.1002/masy.202000247.
[32] J.P. Beaumont, Runner and Gating Design Handbook, second ed., Hanser Gardner Publications, Inc.,, Cincinnati, OH, 2004.
[33] T. Itoh, H. Miyaji, K. Asai, Thermal Properties of α- and γ-Forms of Nylon 6, Jpn. J. Appl. Phys. 14 (1975) 206–215, https://doi.org/10.1143/JJAP.14.206.
[34] N.S. Murthy, S.M. Aharoni, A.B. Szollosi, Stability of the gamma form and the development of the alpha form in nylon 6, Polym. Phys. 23 (1985) 2549–2565, https://doi.org/10.1002/pol.1985.180231212.
[35] X. Zhang, A. Gohn, G. Mendis, J.F. Buzinkai, S.J. Weigand, A.M. Rhoades, Probing three distinct crystal polymorphs of melt-crystallized polyamide 6 by an integrated fast scanning calorimetry chip system, Macromolecules 54 (2021) 7512–7528, https://doi.org/10.1021/acs.macromol.1c00811.
[36] ATEVA 1070 Technical Data Sheet, 2021. https://tools.celanese.com/products/datasheet/SI/ATEVA® 1070 (Accessed 16 August 2021).
[37] E. Parodi, L.E. Govaert, G.W.M. Peters, Glass transition temperature versus structure of polyamide 6: a flash-DSC study, Thermochim. Acta 657 (2017) 110–122, https://doi.org/10.1016/j.tca.2017.09.021.
[38] B. Akhoundi, A.H. Behravesh, Effect of filling pattern on the tensile and flexural mechanical properties of FDM 3D printed products, Exp. Mech. 59 (2019) 883–897, https://doi.org/10.1007/s11340-018-00467-y.
[39] E.A. Papon, A. Haque, Tensile properties, void contents, dispersion and fracture behaviour of 3D printed carbon nanofiber reinforced composites, J. Reinf. Plast. Compos. 37 (2018) 381–395, https://doi.org/10.1177/0731684417750477.
[40] M. Brogly, M. Nardin, J. Schultz, Effect of vinylacetate content on crystallinity and second-order transitions in ethylene-vinylacetate copolymers, J. Appl. Polym. Sci. 64 (1997) 1903–1912, https://doi.org/10.1002/(sici)1097-4628(19970606)64:10<1903::aid-app4>3.3.co;2-s.